

Measurement of the CP observables in $\bar{B}_s^0 \rightarrow D_s^+ K^-$ and first observation of $\bar{B}_{(s)}^0 \rightarrow D_s^+ K^- \pi^+ \pi^-$ and $\bar{B}_s^0 \rightarrow D_{s1}(2536)^+ \pi^-$

Steven R. Blusk

Department of Physics

Syracuse University

Syracuse, NY 13244, USA

Proceedings of CKM 2012, the 7th International Workshop on the CKM Unitarity Triangle, University of Cincinnati, USA, 28th September - 2 October 2012

1 Introduction

A central goal of flavor physics is to measure the angle $\gamma \equiv \arg\left(-\frac{V_{ub}^* V_{ud}}{V_{cb}^* V_{cd}}\right)$ in the Cabibbo-Kobayashi-Maskawa (CKM) [1, 2] mixing matrix, which is currently known to a precision of about 10-12° [3]. The theoretically cleanest methods employ $B \rightarrow DK$ decays, where the sensitivity to γ results from the interference between $b \rightarrow c$ and $b \rightarrow u$ transitions. Since both transitions are $\mathcal{O}(\lambda^3)$ in the Wolfenstein parameter [4], large CP violating asymmetries are expected. One powerful class of methods utilize $B^- \rightarrow DK^-$ where the D is detected in either a CP eigenstate [7], a flavor-specific mode [6], or a multi-body decay [8]. An advantage of these decays is that they do not require knowledge of the b -hadron flavor at production (flavor tagging), and only rely on measuring the time integrated rates. Another powerful method to extract γ is to perform a time-dependent analysis of $\bar{B}_s^0 \rightarrow D_s^+ K^-$ [9, 10, 11] and $\bar{B}_s^0 \rightarrow D_s^+ K^- \pi^+ \pi^-$. Time-dependent analyses of $\bar{B}_s^0 \rightarrow D_s^+ K^- (\pi^+ \pi^-)$ are only possible at hadron colliders, and are a unique capability of LHCb.

The time-dependent decay rates of B_s^0 and \bar{B}_s^0 to a flavor-specific final state,

16 $f = D_s^+ K^-$, is given by:

$$\frac{d\Gamma_{B_s^0 \rightarrow f}(t)}{dt} = \frac{1}{2}|A_f|^2(1 + |\lambda_f|^2)e^{-\Gamma_s t} \left[\cosh\left(\frac{\Delta\Gamma_s t}{2}\right) + D_f \sinh\left(\frac{\Delta\Gamma_s t}{2}\right) + C_f \cos(\Delta m_s t) - S_f \sin(\Delta m_s t) \right] \quad (1)$$

$$\frac{d\Gamma_{\bar{B}_s^0 \rightarrow f}(t)}{dt} = \frac{1}{2}|A_f|^2 \left|\frac{p}{q}\right|^2 (1 + |\lambda_f|^2)e^{-\Gamma_s t} \left[\cosh\left(\frac{\Delta\Gamma_s t}{2}\right) + D_f \sinh\left(\frac{\Delta\Gamma_s t}{2}\right) - C_f \cos(\Delta m_s t) + S_f \sin(\Delta m_s t) \right] \quad (2)$$

17 where A_f is the decay amplitude $A(B_s^0 \rightarrow f)$ and $\lambda_f = (q/p)(\bar{A}_f/A_f) = |\lambda_f|e^{i(\Delta - (\gamma - 2\beta_s))}$.
 18 Here, $|\lambda_f|$ and Δ are the relative magnitude and strong phase difference between the
 19 $b \rightarrow u$ and $b \rightarrow c$ transitions, and $2\beta_s$ is the phase of B_s^0 mixing. The complex coeffi-
 20 cients p and q relate the B_s^0 meson mass eigenstates, $B_{H,L}$, to the flavor eigenstates,
 21 B_s^0 and \bar{B}_s^0 via:

$$\begin{aligned} B_L &= pB_s^0 + q\bar{B}_s^0, \\ B_H &= pB_s^0 - q\bar{B}_s^0, \end{aligned} \quad |p|^2 + |q|^2 = 1. \quad (3)$$

22 Similar equations can be written for the CP -conjugate decays, replacing A_f by $\bar{A}_{\bar{f}} =$
 23 $A(\bar{B}_s^0 \rightarrow \bar{f})$, λ_f by $\bar{\lambda}_{\bar{f}} = (p/q)(A_{\bar{f}}/\bar{A}_{\bar{f}})$, $|p/q|^2$ by $|q/p|^2$, C_f by $C_{\bar{f}}$, S_f by $S_{\bar{f}}$, and D_f
 24 by $D_{\bar{f}}$. The CP asymmetry observables $C_f, S_f, D_f, C_{\bar{f}}, S_{\bar{f}}$ and $D_{\bar{f}}$ are then given by

$$\begin{aligned} C_f = C_{\bar{f}} &= \frac{1 - |\lambda_f|^2}{1 + |\lambda_f|^2}, & S_f &= \frac{2\mathcal{I}m(\lambda_f)}{1 + |\lambda_f|^2}, & D_f &= \frac{2\mathcal{R}e(\lambda_f)}{1 + |\lambda_f|^2}, \\ S_{\bar{f}} &= \frac{2\mathcal{I}m(\bar{\lambda}_{\bar{f}})}{1 + |\bar{\lambda}_{\bar{f}}|^2}, & D_{\bar{f}} &= \frac{2\mathcal{R}e(\bar{\lambda}_{\bar{f}})}{1 + |\bar{\lambda}_{\bar{f}}|^2}. \end{aligned} \quad (4)$$

25 Since CP violation in mixing is expected to be below the percent level, it follows that
 26 $|q/p| = 1$, $|\lambda_f| = |\bar{\lambda}_{\bar{f}}|$, and consequently $C_f = C_{\bar{f}}$. Thus there are five observables
 27 that depend on the 3 physics parameters of interest: $|\lambda_f|$, Δ and $\gamma - 2\beta_s$. Similar
 28 expressions are applicable to $\bar{B}_s^0 \rightarrow D_s^+ K^- \pi^+ \pi^-$, however, there is a potential dilution
 29 due to the varying strong phase across the $D_s^+ K^- \pi^+ \pi^-$ Dalitz plane.

30 In this article, we present the first measurements of these five CP observables.
 31 First observations of the $\bar{B}_s^0 \rightarrow D_s^+ K^- \pi^+ \pi^-$, $\bar{B}^0 \rightarrow D_s^+ K^- \pi^+ \pi^-$ and $\bar{B}_s \rightarrow D_{s1}(2536)^+ \pi^-$
 32 decays are also presented, along with measurements of their relative branching frac-
 33 tions. All results are based on 1.0 fb^{-1} of integrated luminosity recorded in 2011
 34 by the LHCb experiment. More detailed documentation of the $\bar{B}_s^0 \rightarrow D_s^+ K^-$ and
 35 $\bar{B}_{(s)}^0 \rightarrow D_s^+ K^- \pi^+ \pi^-$ analyses can be found in Refs. [12] and [13], respectively.

2 Event Selection

Signal D_s^+ candidates are formed by reconstructing $D_s^+ \rightarrow K^+K^-\pi^+$, $D_s^+ \rightarrow \pi^+\pi^-\pi^+$ and $D_s^+ \rightarrow K^+\pi^-\pi^+$. For the $\bar{B}_s^0 \rightarrow D_s^+K^-\pi^+\pi^-$ and $\bar{B}_s^0 \rightarrow D_s^+\pi^-\pi^+\pi^-$ candidates, only the $D_s^+ \rightarrow K^+K^-\pi^+$ decay is considered. The D_s^+ candidates are required to form a good quality vertex, be spacially well separated from any primary vertex (PV), and have an invariant mass consistent with the known D_s^+ mass (within about 3 times the mass resolution). Multivariate selection algorithms are employed to suppress the combinatorial background, and typically have a signal efficiency of 80-90% while rejecting about 85% of the combinatorial background. Invariant mass distributions for D_s^+ candidates are shown in Fig. 1 for the higher signal yield $\bar{B}_s^0 \rightarrow D_s^+\pi^-$ decay, showing that clean signals are achievable even in the suppressed D_s^+ decay modes. Tighter

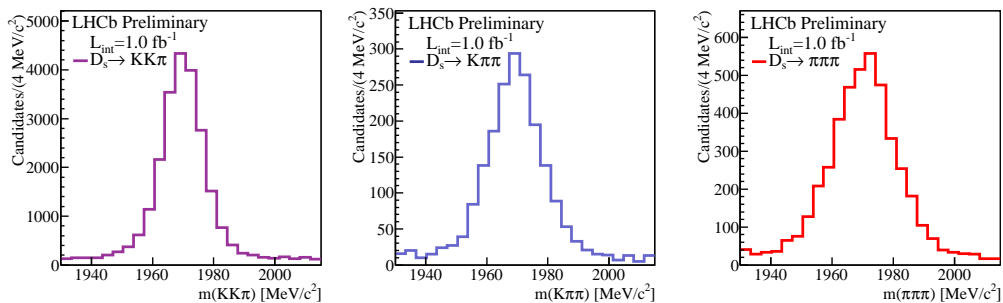


Figure 1: Invariant mass distributions for D_s^+ candidates in the $\bar{B}_s^0 \rightarrow D_s^+\pi^-$ data sample, for (left) $K^+K^-\pi^+$, (middle) $K^+\pi^-\pi^+$, and (right) $\pi^+\pi^-\pi^+$ final states.

particle identification requirements are applied to the K^- or $K^-\pi^+\pi^-$ recoiling from the D_s^+ to suppress cross-feed from the favored $\bar{B}_s^0 \rightarrow D_s^+\pi^-$ and $\bar{B}_s^0 \rightarrow D_s^+\pi^-\pi^+\pi^-$ decays. For the $\bar{B}_s^0 \rightarrow D_s^+\pi^-\pi^+\pi^-$ and $\bar{B}_s^0 \rightarrow D_s^+K^-\pi^+\pi^-$ decays, the invariant mass of the $\pi^-\pi^+\pi^-$ and $K^-\pi^+\pi^-$ systems are restricted to be below 3000 MeV/c².

3 Analysis of $\bar{B}_s^0 \rightarrow D_s^+\pi^-$ and $\bar{B}_s^0 \rightarrow D_s^+K^-$

The invariant mass distributions for $\bar{B}_s^0 \rightarrow D_s^+\pi^-$ and $\bar{B}_s^0 \rightarrow D_s^+K^-$ are shown in Figs. 2 and 3. All three D_s^+ decay modes have approximately equal B_s^0 mass resolutions, and are summed together in these distributions. The signal shape is modeled as the sum of two Crystal Ball [14] functions, with one exponential tail on each side of the \bar{B}_s^0 signal peak. A number of specific backgrounds, due to either a missed particle (e.g. $\bar{B}_s^0 \rightarrow D_s^+\rho^-$, with the π^0 undetected), a misidentified particle (e.g. $\bar{B}_s^0 \rightarrow D_s^+\pi^-$ reconstructed as $\bar{B}_s^0 \rightarrow D_s^+K^-$), or both (e.g. $\bar{B}_s^0 \rightarrow D_s^+\rho^-$

59 reconstructed as $\bar{B}_s^0 \rightarrow D_s^+ K^-$) are accounted for using either data or simulation
 60 to model the shape of these backgrounds. From an unbinned extended maximum
 61 likelihood fit, $27,965 \pm 395 \bar{B}_s^0 \rightarrow D_s^+ \pi^-$ and $1390 \pm 98 \bar{B}_s^0 \rightarrow D_s^+ K^-$ signal events
 are selected. The CP parameters are obtained by a fit to the decay time distribution

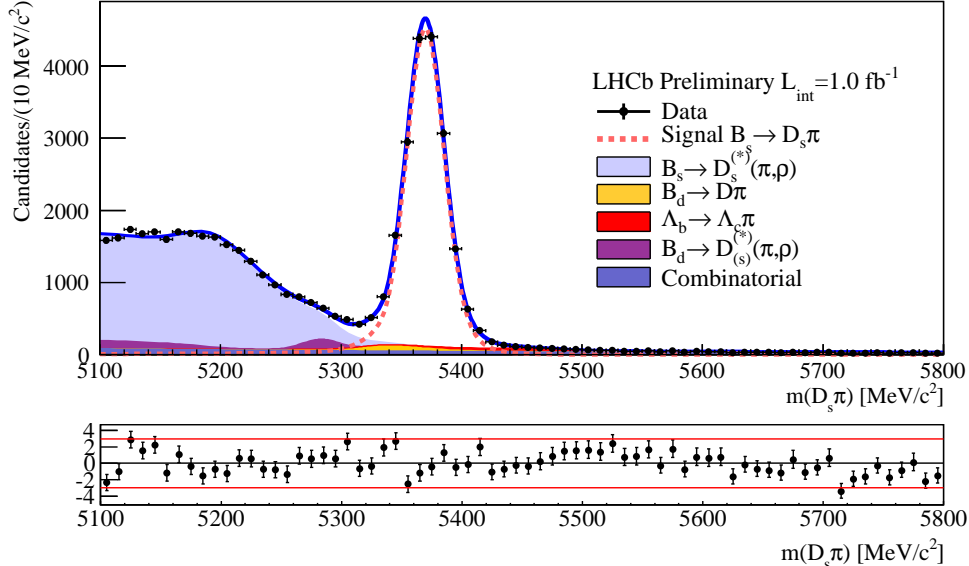


Figure 2: Invariant mass distributions $\bar{B}_s^0 \rightarrow D_s^+ \pi^-$ candidates. The signal component is indicated by the dashed curve, and the backgrounds are indicated by the various color-filled (shaded, in B/W) curves.

62 of the $\bar{B}_s^0 \rightarrow D_s^+ K^-$ signal candidates. Two methods have been developed. The first,
 63 referred to as *sFit*, uses *sWeights* [15] obtained from the $\bar{B}_s^0 \rightarrow D_s^+ K^-$ mass fit to
 64 statistically subtract the background contribution. The second method, referred to
 65 as *cFit*, is a conventional two-dimensional fit to the reconstructed mass and decay
 66 time. The advantage of the first method is that there is no need to model the time
 67 distribution of all the backgrounds, as they are statistically removed via the *sWeights*.
 68 The statistical subtraction, as presented here, uses events in the full mass fit region,
 69 and the subtraction of this background leads to a larger statistical uncertainty than
 70 if just a narrow signal region is used. For this reason, the second method is expected
 71 to give a smaller statistical uncertainty; however it requires an accurate model of
 72 the time distributions of the backgrounds that enter into the signal region. For the
 73 analysis presented here, the *sFit* provides the nominal result, and the *cFit* is used as
 74 a cross-check.

76 The measurement of the CP parameters in $\bar{B}_s^0 \rightarrow D_s^+ K^-$ requires a fit to the time-
 77 dependent decay rates. The fit accounts for (i) the acceptance versus reconstructed
 78 decay time, (ii) the decay time resolution, and (iii) the effective tagging efficiency. The

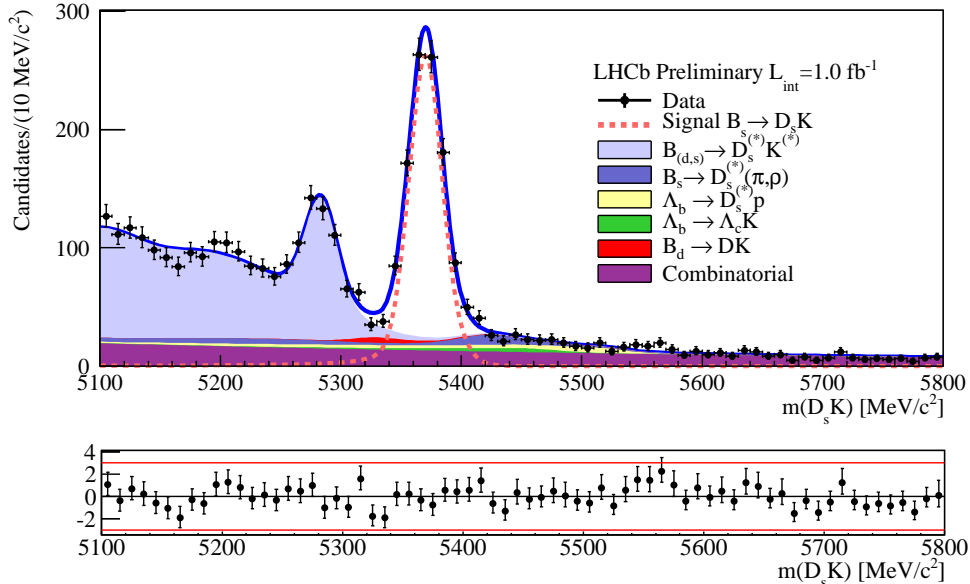


Figure 3: Invariant mass distributions $\bar{B}_s^0 \rightarrow D_s^+ K^-$ candidates. The signal component is indicated by the dashed curve, and the backgrounds are indicated by the various color-filled (shaded, in B/W) curves.

79 functional form of the acceptance function is determined from simulated $\bar{B}_s^0 \rightarrow D_s^+ \pi^-$,
80 and its parameters are determined in a fit to $\bar{B}_s^0 \rightarrow D_s^+ \pi^-$ data, where the B_s^0 lifetime
81 and mixing frequency, Δm_s , are fixed to 1.51 ps and 17.69 ps⁻¹ [17], respectively.
82 The average decay time resolution is about 50 fs, and is modeled by the sum of
83 three Gaussian functions, whose parameters are determined from simulation. The
84 Gaussian width parameters obtained from simulation are scaled up by 1.15 to account
85 for better resolution in the simulation than in data; this factor is determined by
86 comparing the width of the zero decay time component of prompt D_s^+ plus one random
87 track in data and simulation. For the flavor tagging, only *opposite side* (OS) taggers
88 are currently used. These algorithms exploit the correlation in flavor between the
89 signal b hadron at production, and the other b hadron in the event (referred to as
90 the tag- b). In particular, the charge of either an electron, a muon, or a kaon that
91 does not come from any pp interaction vertex (or the signal b), or the charge of
92 another secondary vertex in the event, provide information on the flavor of the tag- b
93 hadron. Because $b\bar{b}$ are produced in pairs, this translates into a flavor determination
94 of the signal B_s^0 . The OS flavor tagging algorithm was initially tuned using simulated
95 decays, and then re-optimized and calibrated to obtain the largest effective tagging
96 efficiency using the self-tagging $B^+ \rightarrow J/\psi K^+$ and $B^0 \rightarrow D^{*-} \mu^+ \nu$ decays in data. In
97 general, the performance of the OS tagging algorithms are independent of the signal
98 b -hadron decay, and have a combined effective tagging efficiency of $\epsilon D^2 = 1.90\%$ for

99 $\bar{B}_s^0 \rightarrow D_s^+ K^-$. Further details of the tagging algorithms can be found in Ref [16].

100 In the fit to $\bar{B}_s^0 \rightarrow D_s^+ K^-$, the following parameters are fixed: $\Delta m_s = 17.69 \text{ ps}^{-1}$,
 101 $\tau_{B_s} = 1.51 \text{ ps}$ and $\Delta\Gamma_s \equiv \Gamma_{s,L} - \Gamma_{s,H} = 0.105 \text{ ps}^{-1}$ [17]. About 60% of the
 102 $\bar{B}_s^0 \rightarrow D_s^+ K^-$ candidates have no flavor tag; the time-dependent decay rates for
 103 these untagged decays is given by the sum of the two expressions in Eq. 3, and
 104 the sensitivity to γ enters through the hyperbolic sine term. The decay time distri-
 105 bution of $\bar{B}_s^0 \rightarrow D_s^+ K^-$ signal decays and projections of the fitted are shown in
 106 Fig. 4. The projections show the four possible tagged decays, $B_s^0 \rightarrow D_s^\pm K^\mp$ and
 107 $\bar{B}_s^0 \rightarrow D_s^\pm K^\mp$, as well as the untagged time-dependent decay rates (B_s^0, \bar{B}_s^0) $\rightarrow D_s^- K^+$
 and (B_s^0, \bar{B}_s^0) $\rightarrow D_s^+ K^-$. The fitted values for the CP parameters are

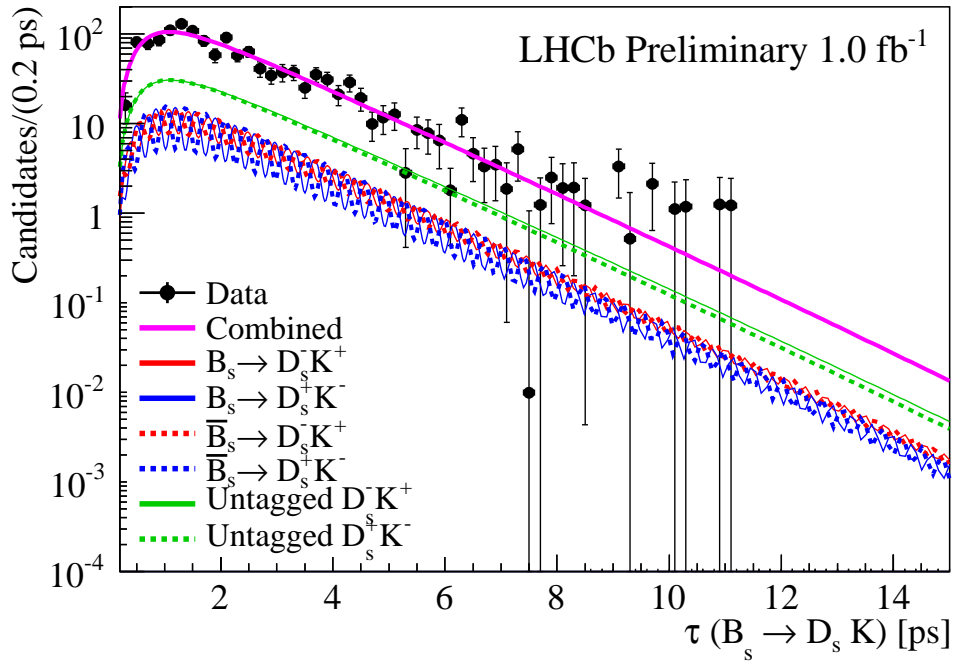


Figure 4: Distribution of reconstruct decay time for $\bar{B}_s^0 \rightarrow D_s^+ K^-$ signal decays (points with error bars), along with the results of the fit. Projections of the decay rates versus the decay time for the four possible flavor tagged decays, and the two untagged decays.

$$\begin{aligned}
C &= 1.01 \pm 0.50 \pm 0.23, \\
S_f &= -1.25 \pm 0.56 \pm 0.24, \\
S_{\bar{f}} &= 0.08 \pm 0.68 \pm 0.28, \\
D_f &= -1.33 \pm 0.60 \pm 0.26, \\
D_{\bar{f}} &= -0.81 \pm 0.56 \pm 0.26,
\end{aligned}$$

109 where the first uncertainties are statistical and the second are systematic. Several
110 sources of systematic uncertainty have been considered. The dominant sources are
111 due to the precision on the effective flavor tagging efficiency ($0.16\sigma_{\text{stat}}-0.23\sigma_{\text{stat}}$), vari-
112 ations in the parameters that are fixed in the default fits ($0.15\sigma_{\text{stat}}-0.42\sigma_{\text{stat}}$), and
113 the correlation between the mass of specific backgrounds and their reconstructed de-
114 cay time ($0.08\sigma_{\text{stat}}-0.27\sigma_{\text{stat}}$), where these uncertainties are expressed as a fraction
115 of the statistical error. These are the first measurements of the CP parameters in
116 $\bar{B}_s^0 \rightarrow D_s^+ K^-$. With additional data and analysis refinements, reduction in both the
117 statistical and systematic uncertainties are expected.

118 4 First observation of $\bar{B}_s \rightarrow D_s^+ K^- \pi^+ \pi^-$ and $\bar{B}_s^0 \rightarrow$ 119 $D_{s1}(2536)^+ \pi^-$

120 The decay $\bar{B}_s^0 \rightarrow D_s^+ K^- \pi^+ \pi^-$ can be analyzed in a similar way to $\bar{B}_s^0 \rightarrow D_s^+ K^-$ to
121 measure the weak phase γ . While this decay has not yet been observed, if one uses
122 \bar{B}^0 and B^- decays as a guide, it would naively be expected that its branching fraction
123 is 1.5-2.0 times larger than $\bar{B}_s^0 \rightarrow D_s^+ K^-$, making this a potentially attractive decay
124 mode to explore. The first step in such an analysis is to firmly establish an observation
125 of this decay and measure its branching fraction (here, relative to $\bar{B}_s^0 \rightarrow D_s^+ \pi^- \pi^+ \pi^-$).
126 While searching for this decay, the decay $\bar{B}_s^0 \rightarrow D_s^+ K^- \pi^+ \pi^-$ is also observed and its
127 branching fraction is measured relative to $\bar{B}_s^0 \rightarrow D_s^+ K^- \pi^+ \pi^-$.

128 With the previously defined selections, Fig. 5 shows the invariant mass distri-
129 butions for (left) $\bar{B}_s^0 \rightarrow D_s^+ \pi^- \pi^+ \pi^-$ candidates and (right) $\bar{B}_{(s)}^0 \rightarrow D_s^+ K^- \pi^+ \pi^-$
130 candidates. Significant \bar{B}_s^0 signals are seen in both spectra, and a \bar{B}^0 signal is seen
131 in the $D_s^+ K^- \pi^+ \pi^-$ mass distribution. The main sources of background are $\bar{B}_s^0 \rightarrow$
132 $D_s^{*+} \pi^- \pi^+ \pi^-$ (to $\bar{B}_s^0 \rightarrow D_s^+ \pi^- \pi^+ \pi^-$), and $\bar{B}_s^0 \rightarrow D_s^+ \pi^- \pi^+ \pi^-$, $\bar{B}_s^0 \rightarrow D_s^{*+} \pi^- \pi^+ \pi^-$,
133 and $\bar{B}_{(s)}^0 \rightarrow D_s^{*+} K^- \pi^+ \pi^-$ (to $\bar{B}_{(s)}^0 \rightarrow D_s^+ K^- \pi^+ \pi^-$). Their shapes are taken from
134 simulation, with parameters that are allowed to vary within their uncertainties.
135 Yields of 5683 ± 83 $\bar{B}_s^0 \rightarrow D_s^+ \pi^- \pi^+ \pi^-$, 216 ± 21 $\bar{B}_s^0 \rightarrow D_s^+ K^- \pi^+ \pi^-$ and 402 ± 33
136 $\bar{B}^0 \rightarrow D_s^+ K^- \pi^+ \pi^-$ are observed. After correcting for the relative efficiencies, the ratio

137 of branching fractions are measured to be

$$\frac{\mathcal{B}(\bar{B}_s^0 \rightarrow D_s^+ K^- \pi^+ \pi^-)}{\mathcal{B}(\bar{B}_s^0 \rightarrow D_s^+ \pi^- \pi^+ \pi^-)} = (5.2 \pm 0.5 \pm 0.3) \times 10^{-2}$$

$$\frac{\mathcal{B}(\bar{B}^0 \rightarrow D_s^+ K^- \pi^+ \pi^-)}{\mathcal{B}(\bar{B}_s^0 \rightarrow D_s^+ K^- \pi^+ \pi^-)} = 0.54 \pm 0.07 \pm 0.07,$$

where the uncertainties are statistical and systematic, respectively. These are the

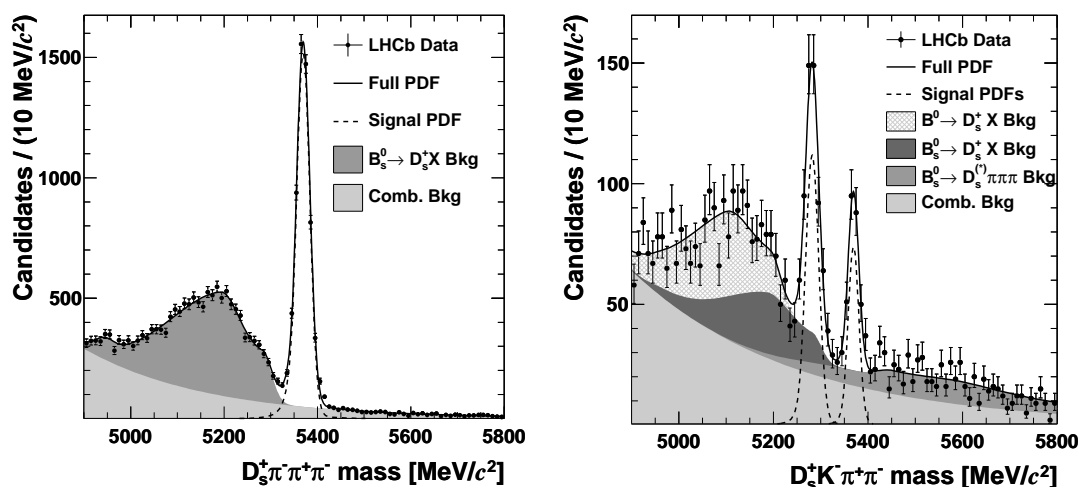


Figure 5: Invariant mass distribution for (left) $\bar{B}_s^0 \rightarrow D_s^+ \pi^- \pi^+ \pi^-$ candidates and (right) $\bar{B}_{(s)}^0 \rightarrow D_s^+ K^- \pi^+ \pi^-$ candidates. The fitted signal (dashed lines) and background shapes (shaded/hatched regions) are shown, as described in the text.

138

139 first observations of these decays. Since $\bar{B}_s^0 \rightarrow D_s^+ \pi^- \pi^+ \pi^-$ has a branching fraction
 140 that is about twice as large as $\bar{B}_s^0 \rightarrow D_s^+ \pi^-$, and $\mathcal{B}(\bar{B}_s^0 \rightarrow D_s^+ K^-) \sim 0.09 \times \mathcal{B}(\bar{B}_s^0 \rightarrow$
 141 $D_s^+ \pi^-)$ [18], it follows that $\mathcal{B}(\bar{B}_s^0 \rightarrow D_s^+ \pi^- \pi^+ \pi^-)$ is at least as large as $\mathcal{B}(\bar{B}_s^0 \rightarrow$
 142 $D_s^+ \pi^-)$, or as much as 50% larger. The $\mathcal{B}(\bar{B}^0 \rightarrow D_s^+ K^- \pi^+ \pi^-)$ is also sizeable, and is
 143 likely dominated by contributions where an extra $s\bar{s}$ pair is produced in addition to
 144 the weak decay (see Ref. [13] for more details).

145 The $\bar{B}_s^0 \rightarrow D_s^+ \pi^- \pi^+ \pi^-$ decay has also been analyzed to search for intermediate
 146 excited D_{sj} states. For $\bar{B}_s^0 \rightarrow D_s^+ \pi^- \pi^+ \pi^-$ candidates within 40 MeV/ c^2 of the \bar{B}_s^0
 147 signal peak, the mass difference, $\Delta M \equiv M(D_s^+ \pi^- \pi^+) - M(D_s^+)$ is computed for both
 148 $\pi^- \pi^+$ mass combinations. The resulting mass difference spectrum is shown in Fig. 6.
 149 The signal is fit with a Breit-Wigner convolved with a Gaussian resolution function

150 whose width is fixed to the expected ΔM resolution. A signal of 20.0 ± 5.1 events is
 151 observed with a ΔM value and width consistent with the $D_{s1}(2536)^+$ state. Applying
 152 corrections for the relative efficiency, the ratio of branching fractions is measured to
 153 be

$$\frac{\mathcal{B}(\bar{B}_s^0 \rightarrow D_{s1}(2536)^+ \pi^-, D_{s1}^+ \rightarrow D_s^+ \pi^- \pi^+)}{\mathcal{B}(\bar{B}_s^0 \rightarrow D_s^+ \pi^- \pi^+ \pi^-)} = (4.0 \pm 1.0 \pm 0.4) \times 10^{-3}.$$

154 The excess of events is 5.9 standard deviations over the expected background, thus
 establishing the first observation of this decay.

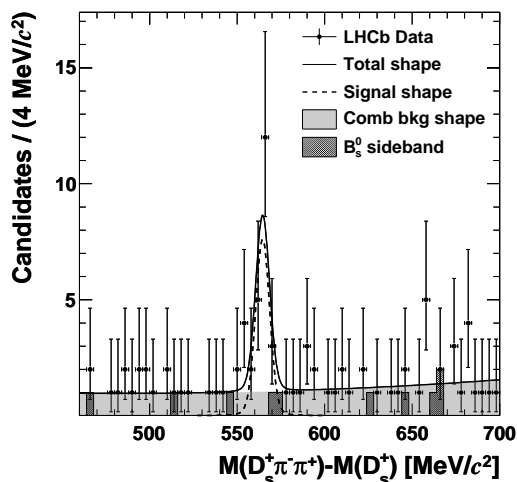


Figure 6: Distribution of the difference in invariant mass, $M(D_s^+ \pi^- \pi^+) - M(D_s^+)$, using $\bar{B}_s^0 \rightarrow D_s^+ \pi^- \pi^+ \pi^-$ candidates within $40 \text{ MeV}/c^2$ of the known B_s^0 mass (points) and in the upper B_s^0 mass sidebands (filled histogram). The fit to the distribution is shown, as described in the text.

155

156 5 Summary

157 First measurements of the CP observables in the $\bar{B}_s^0 \rightarrow D_s^+ K^-$ decay have been re-
 158 ported. With the larger data sample recorded in 2012, and the larger data set antici-
 159 pated in the future, this decay will contribute significantly to the determination of the
 160 weak phase γ . First observations of the $\bar{B}_s^0 \rightarrow D_s^+ K^- \pi^+ \pi^-$ and $\bar{B}^0 \rightarrow D_s^+ K^- \pi^+ \pi^-$
 161 are also reported. The former can be used in a similar way to $\bar{B}_s^0 \rightarrow D_s^+ K^-$ to

162 extract γ . After including $D_s^+ \rightarrow \pi^+\pi^-\pi^+$ and $D_s^+ \rightarrow K^-\pi^+\pi^-$ decays, and re-
163 optimizing the selection for $\bar{B}_s^0 \rightarrow D_s^+K^-\pi^+\pi^-$ only, the yield in this mode more
164 than doubles with a comparable signal-to-background. The yield in this mode is
165 therefore expected to have about 35-40% of that obtained in $\bar{B}_s^0 \rightarrow D_s^+K^-$. The
166 $\bar{B}_s^0 \rightarrow D_{s1}(2536)^+\pi^-$ decay is also observed for the first time, and its branching frac-
167 tion relative to $\bar{B}_s^0 \rightarrow D_s^+\pi^-\pi^+\pi^-$ is presented.

168 Acknowledgements

169 I gratefully acknowledge support from the National Science Foundation, which makes
170 this research possible.

171 References

- 172 [1] N. Cabibbo, Phys. Rev. Lett. **10**, 531 (1963).
173 [2] M. Kobayashi and T. Maskawa, Prog. Theor. Phys. **49**, 652 (1973).
174 [3] See talks by G. Eigen and D. Derkach in these proceedings; Also, see S. Descotes-
175 Genon *et al.* (CKMFitter collaboration), Proceedings Supplements, Capri, Italy,
176 July 11-13, 2012, to be published in Nucl. Phys. **B**. Updated results and plots
177 available at: <http://ckmfitter.in2p3.fr>; Also, M. Bona (UTFit collaboration),
178 Proceedings Supplements, Capri, Italy, July 11-13, 2012, to be published in
179 Nucl. Phys. **B**, with updated results at <http://www.utfit.org/UTFit>.
180 [4] L. Wolfenstein, Phys. Rev. Lett. **51**, 1945 (1983).
181 [5] See contributions by S. Malde and M. John, these proceedings.
182 [6] D. Atwood, G. Eilam, M. Gronau, and A. Soni, Phys. Lett. **B341**, 372 (1995).
183 [7] M. Gronau and D. London, Phys. Lett. **B253**, 483 (1991); M. Gronau and
184 D. Wyler, Phys. Lett. **B265**, 172 (1991).
185 [8] A. Giri, Y. Grossman, A. Soffer, and J. Zupan, Phys. Rev. **D68**, 054018 (2003).
186 [9] R. Aleksan, I. Dunietz and B. Kayser, Z. Phys. **C54**, 653 (1992).
187 [10] R. Fleischer, Nucl. Phys. **B671**, 459 (2003).
188 [11] K. De Bruyn, R. Fleischer, R. Knegjens, M. Merk, M. Schiller and N. Tuning,
189 Nucl. Phys. **B868**, 351 (2012).
190 [12] LHCb collaboration, LHCb-CONF-2012-029.

- 191 [13] R. Aaij (LHCb collaboration), LHCb-PAPER-2012-033, arXiv:1211.1541, sub-
192 mitted to Phys. Rev. **D**.
- 193 [14] T. Skwarnicki, PhD thesis, Institute of Nuclear Physics, Krakow, 1986, DESY-
194 F31-86-02.
- 195 [15] M. Pivk and F. R. Le Diberder, Nucl. Instrum. Meth. **A555**, 356 (2005).
- 196 [16] R. Aaij et. al. (LHCb Collaboration), Eur. Phys. J. **C72**, 2022 (2012); LHCb-
197 CONF-2012-026; Also see contribution by J. Wishahi in these proceedings.
- 198 [17] Heavy Flavor Averaging Group, D. Asner et al., Averages of b-hadron,
199 chadron, and tau-lepton Properties, arXiv:1010.1589, Online updates available
200 at <http://www.slac.stanford.edu/xorg/hfag/>.
- 201 [18] Particle Data Group, J. Beringer *et al.*, Phys. Rev. **D86**, 010001 (2012).